Batch adsorption studies on the removal of malachite green from water by chemically modified *Azolla pinnata*

Muhammad Raziq Rahimi Kooh*, Linda B.L. Lim, Lee Hoon Lim, J.M.R.S. Bandara

Faculty of Science, Universiti Brunei Darussalam, Jalan Tungku Link, Pengkalan Gadong, Bandar Seri Begawan BE 1410, Brunei Darussalam, Tel. +673 8658876; emails: chernyuan@hotmail.com (M.R.R. Kooh), linda.lim@ubd.edu.bn (L.B.L. Lim), leehoon.lim@ubd.edu.bn (L.H. Lim), bandara.sarath@gmail.com (J.M.R.S. Bandara)

ABSTRACT

Azolla pinnata (AP), a common water fern found in rice fields in Asia and cultivated for biological nitrogen fixation, was studied as a potential adsorbent for the removal of malachite green in a batch adsorption system. The batch adsorption studies, involving unmodified AP (UAP) and two chemically modified AP—H_3PO_4-treated AP (PAP) and NaOH-treated AP (NAP)—included the effects of adsorbent dosage, pH, ionic strength, contact time, thermodynamics and kinetics studies, estimation of activation energy and regeneration experiments. Three isotherm models namely the Langmuir, Freundlich and Dubinin–Radushkevich models were used and the Langmuir model best represented all the three adsorption systems with maximum adsorption capacity (q_m) of UAP, PAP and NAP at 25°C, to be at 87.0, 292.1 and 109.6 mg g^{-1}, respectively. The kinetics modelling included the pseudo-first-order, pseudo-second-order, Weber–Morris intraparticle diffusion and the Boyd models. Thermodynamic studies showed that all the three adsorption systems are endothermic and spontaneous in nature. All three adsorbents were regenerated with 0.1 mol L^{-1} NaOH and were effective even after five cycles.

Keywords: Malachite green dye; *Azolla pinnata*; Adsorption isotherm; Chemically modified adsorbent; Kinetics; Thermodynamics

1. Introduction

Synthetic dyes have become irreplaceable in the modern lifestyle. Their applications range from dyeing textiles, printing and process of tanning and dyeing leather to food colouring agents. Point pollution caused by discharging dye wastewater to open water bodies leads to the destruction of aquatic ecosystems and often contamination of food web. One of the significant reasons is the destruction of aesthetic values

due to the high extinction coefficient of dyes where their vibrant colours can be observed even at low concentrations of dye. This reduces sunlight penetration into the water, thereby reducing photosynthetic activities of aquatic plant and algae leading to the reduction of dissolved oxygen levels.

This study investigates a hazardous water-soluble dye, malachite green (MG), belonging to the triphenylmethane family, and is widely used to dye wool, leather, silk and cotton [1]. Apart from colouring purposes, MG is also widely used in aquaculture and animal feeds mainly for its antifungal, antiparasitic and

*Corresponding author.

antiseptic properties [2,3]. The toxic MG residues can also be bio-accumulated in fish and aquatic fauna resulting in transfer of pollutants higher up the food chain [2]. Animal testing on fish (*Ictalurus punctatus*) reported a LC_{50} at 0.14 mg L^{-1} [4]. MG is also a suspected human reproductive toxicant and a severe eye irritant [4].

Many textile processing industries are located in rural areas where drainage of dyes to municipal sewerage treatment increases the costs of wastewater treatment [5]. This is because municipal sewerage systems utilise an aerobic treatment process, which is dependent on biological processes, and have been proven inefficient to treat dye wastewater [6].

There are many effective dye wastewater treatment methods that have been innovated and improved upon over the years. Some of these methods include the uses of reducing or oxidising agents, ozonation, Fenton's reagent, electrochemical oxidation [7], reverse osmosis, ion exchange [8] and adsorption. The advantages and disadvantages of these methods are widely discussed in literature [9–12].

Adsorption is one of the preferred methods for wastewater treatment due to its simple design, where semi-skilled workers can learn to effectively treat the dye wastewater without needing to possess advanced knowledge. The choice of adsorbents ranges from low-cost materials such as agriculture wastes e.g. walnut shells [13], egg shell [14,15], hen feather [1,16–18], soya waste [19], bottom ash [20], plant fibre [21] and fruit wastes [22–25], and soil materials such as peat [26], to more expensive options such as activated carbon. The use of low-cost adsorbents can increase the affordability of small industries to treat the wastewater.

This research work aims to investigate the use of a species of water fern, *Azolla pinnata* (AP), as a potential adsorbent for the removal of MG. AP has been used in many Asian countries as green manure to fertilise paddy fields, as animal feed, and is widely available in many other countries [27]. AP is invasive and known to cover water bodies within a short duration of time. AP carries a symbiotic nitrogen-fixing cyanobacterium *Anaebaena azollae* that fixes nitrogen from the atmosphere which meet the nitrogen requirements for growth and reproduction of the host. The abundance and availability of AP are two of the reasons that AP is the adsorbent of choice for this study. *Azolla* was reported to contain lignocellulosic materials [27], which is a known precursor that can be chemically modified to remediate water [28]. Many studies on AP were carried out with living samples by phytoremediation method for the removal of heavy metal pollutants such as Hg, Cd, Zn and Pb [29,30], while limited adsorption studies have been reported using

non-living AP samples for the removal of pollutants such as Cd [31] and methyl violet 2B [32].

The objectives of this study are to evaluate the ability of unmodified and chemical-modified AP in the removal of toxic MG based on parameters such as adsorbent dosage, contact time, dye concentration, pH and ionic strength. Phosphoric acid treatment of adsorbent has been known to impregnate phosphate groups to adsorbent's surface [33], while modification with NaOH removed natural fats, waxes and low-molecular weight lignin compounds from the adsorbent's surface, exposing chemical-reactive functional groups, such as the hydroxyl groups [34]. The study was substantiated with thermodynamics, kinetics and regeneration experiments.

2. Materials and methods

2.1. Preparation of stock solution

MG oxalate ($C_{23}H_{25}N_2 \cdot C_2HO_4 \cdot 0.5C_2H_2O_4$, Mr 463.50) of 90% dye content was purchased from Sigma Aldrich Corporation. A stock solution of MG (1,000 mg L^{-1}) was prepared and desired concentrations were obtained by a process of serial dilution. All chemicals were used as received.

2.2. Preparation of adsorbents

A batch of AP was obtained from the Agriculture Department, Ministry of Industrial and Primary Resources, Brunei Darussalam. It was washed with distilled water and oven-dried at 70°C until a constant weight was obtained. The dried samples were ground to fine powder and sieved to particle size of less than 355 μm and stored in a desiccator. This unmodified AP was labelled as UAP.

The phosphoric acid-treated AP (PAP) was prepared by adding 20 g of UAP to 200 mL of 85% *ortho*-phosphoric acid (analysis grade, Merck), shaken in an orbital shaker for 2 h and left to incubate at room temperature for 48 h. PAP was repeatedly washed with 0.05 mol L^{-1} NaHCO$_3$ to neutralise the excess acid, followed by washing with distilled water until the pH was near neutral.

The NaOH-modified AP (NAP) was prepared according to the procedures used by Chieng et al. and with some modifications [35]. Briefly, 20 g of UAP was mixed with 200 mL of 0.5 mol L^{-1} NaOH and shaken in an orbital shaker for 30 min. The modified sample was subjected to 4% (v/v) acetic acid washing to remove excess base, followed by washing with distilled water until the pH was near neutral.

2.3. Characterisation of adsorbents

Elemental analyses were done by X-ray fluorescence (XRF) spectrophotometer (PANalytical Axios^{max}). FTIR spectra of the adsorbents were obtained by using a Shimadzu Model IRPrestige-21 FTIR spectrophotometer.

The point of zero charge (pH$_{pzc}$) of the adsorbents was determined by the salt addition method using 0.1 mol L^{-1} KNO$_3$ solutions [36]. Aliquots of 20 mL KNO$_3$ solutions were adjusted to initial pH values varying between 2.5 and 10.0 with 0.1 mol L^{-1} HNO$_3$ and 0.1 mol L^{-1} NaOH. The pH was measured using Thermo Scientific Orion 2 Star pH Benchtop. Precise quantity of 0.03 g of adsorbent was then added to each aliquot of KNO$_3$ and agitated for 24 h at 250 rpm using a Stuart orbital shaker, and the final pH was measured. The ΔpH (final pH − initial pH) vs. initial pH was plotted to determine the pH$_{pzc}$ (plot not shown for brevity).

2.4. Batch adsorption studies

The batch adsorption studies were carried out by agitating 0.03 g of adsorbent with 20 mL of known concentration of MG in 150 mL Erlenmeyer flasks using a Stuart orbital shaker set at an agitation speed of 250 rpm. Mixtures were agitated for 150 min unless otherwise stated. Batch adsorption studies including the effects of dosage (0.01–0.06 g), contact time (5–240 min), initial concentration C_i (20–600 mg L^{-1}), pH (3.1–6.5), temperature (ambient, 35, 45, 55 and 65°C) and ionic strength (0–0.80 mol L^{-1}) were investigated. The mixture was filtered and the filtrate was analysed using a Shimadzu UV-1601PC UV–visible spectrophotometer at wavelength, λ_{max}, of 618 nm. Duplicates were carried out for all experiments.

2.5. Error analysis

The values of the coefficient of determination (R^2) were used for the determination of the isotherm and kinetics models that best fit the experimental data. The data were further reinforced with four error functions: sum of absolute error (EABS), *Chi*-square test (χ^2), average relative error (ARE) and Marquardt's percent standard deviation (MPSD). Smallest error value indicates the least error [37].

The equations of the four types of error functions were represented as followed:

$$\text{EABS}: \ \sum_{i=1}^{n} \left| q_{e,exp} - q_{e,cal} \right| \tag{1}$$

$$\chi^2: \ \sum_{i=1}^{n} \frac{(q_{e,exp} - q_{e,cal})^2}{q_{e,exp}} \tag{2}$$

$$\text{ARE}: \ \frac{100}{n} \sum_{i=1}^{n} \left| \frac{q_{e,exp} - q_{e,cal}}{q_{e,exp}} \right|_i \tag{3}$$

$$\text{MPSD}: \ 100 \sqrt{\frac{1}{n-p} \sum_{i}^{n} \left(\frac{q_{e,exp} - q_{e,cal}}{q_{e,exp}} \right)^2} \tag{4}$$

where $q_{e,exp}$ is the amount of adsorbate in adsorbent at equilibrium obtained experimentally while $q_{e,cal}$ is the calculated value of q_e using formula of isotherm or kinetic models, n is the total number of data points in the experiment and p is the number of parameters of the model.

2.6. Regeneration studies

The regeneration capability of the adsorbents was studied using three different solvents namely distilled water, 0.1 mol L^{-1} HNO$_3$ and 0.1 mol L^{-1} NaOH, according to methods previously described by Dahri et al. [13]. Briefly, MG-treated adsorbents were obtained by adding the adsorbent to 100 mg L^{-1} MG at the adsorbent dosage of 0.15 g in 100 mL dye. Desorption of the dye from MG-treated adsorbent was achieved by continuous agitation of the dye-treated adsorbent in solvent for 30 min followed by washing several times with distilled water until no further desorption of the dye is visible. The acid and basic washing was continued until the pH of the washed solution approached neutral. The washed adsorbent was dried on a petri dish in an oven at 70°C to be used for the next cycle. Regeneration experiment was carried out for five cycles.

3. Results and discussion

3.1. Characterisations of adsorbents

3.1.1. XRF analysis

The XRF elemental analyses of the adsorbents, before and after dye treatment, are summarised in Table 1. By comparing the adsorbents before dye treatment, PAP displayed a higher amount of elemental P at 3.5% as compared to UAP (2.5%) and NAP (1.0%). This confirmed the loading of phosphate group into the modified adsorbent. The increase of O in PAP (36.4%) and NAP (34.4%) from 28.5% may hint the possibility of the adsorbent's surface to contain more

Table 1
XRF elemental analyses of adsorbents before and after dye treatment

Element	Normalised percentage (%)					
	UAP	UAP-MG	PAP	PAP-MG	NAP	NAP-MG
Al	0.5	0.4	0.4	0.5	0.6	0.4
Mn	0.5	0.3	0.2	0.3	0.9	0.2
Si	1.2	1.8	3.4	3.8	2.6	1.9
P	2.5	1.1	3.5	1.2	1.0	0.8
S	3.6	2.7	5.3	6.2	3.2	3.9
Mg	3.7	1.1	0.7	0.2	5.6	1.6
Na	4.4	ND	20.9	2.8	4.4	0.3
Cl	8.7	0.8	0.9	0.7	0.2	0.8
Fe	6.6	42.4	27.3	44.7	26.8	40.3
Ca	12.3	15.3	0.7	2.3	18.9	15.7
K	14.4	0.2	0.2	0.4	1.4	0.1
O	28.5	33.2	36.4	36.9	34.4	34.1

Note: ND—not detected.

OH or COOH groups. The high Na content (20.9%) of PAP could be a result from the rinsing using $NaHCO_3$. Upon dye treatments, all adsorbents showed a decrease of Na to low levels. The reduction of Na was observed in other biomass adsorbents used in the removal of basic dyes [38–40]. Chieng et al. suggested the possibility of cationic MG molecules which may replace Na^+ during the adsorption process [35].

3.1.2. FTIR analysis

The FTIR spectrum of UAP shows the presence of functional groups: O–H and amine groups (3,360 cm^{-1}), C–H stretch (2,918 and 2,851 cm^{-1}), C=O bending (1,649 cm^{-1}), phenyl (1,442 cm^{-1}) and C–O–C (1,029 cm^{-1}). These functional groups are also present in PAP and NAP, with some slight shifts of bands e.g. for PAP, the C=O and C–O–C bands shifted to 1,651 and 1,026 cm^{-1}, while for NAP, these bands were shifted to 1,641 and 1,030 cm^{-1}, respectively. After dye treatment, shifts were observed for O–H, amine and C–O–C bands, which indicate the possibilities of these groups playing a role in the adsorption of MG. FTIR spectra of all the three dye-treated adsorbents showed additional bands of –COO^- anti-symmetric stretching at 1,585 cm^{-1}, –COO^- symmetric stretching (1,369–1,370 cm^{-1}) and C–N stretching of MG (1,159–1,170 cm^{-1}). These new bands confirm the loading of MG dye onto the adsorbents, and suggest –COO^- may be involved in the interaction with MG molecules [41].

3.2. Effect of adsorbent dosage

The effect of adsorbent dosage for UAP and NAP was conducted at a dye concentration of 100 mg L^{-1}, while 400 mg L^{-1} MG was used for PAP. This is because the concentration at 100 mg L^{-1} dye is insufficient for PAP due to its higher adsorption capacity, where the adsorbent dosage of 0.02–0.06 g resulted in high dye removal ≥97%. A gradual increase in the percentage removal of MG was observed as the dosage increased. Adsorbent dosage beyond 0.03 g resulted in a small increase in MG removal, while the dosage of 0.03 g was effectively high enough for dye removal; thus, this dosage was used for the rest of the experiments for all the three adsorbents.

3.3. Effects of pH and ionic strength

The three major attraction forces responsible for the adsorption of dye are electrostatic interaction, hydrophobic–hydrophobic interaction and hydrogen bonding [42,43]. The study of the effect of pH is important as electrostatic iteration is mainly affected by pH (protonation and deprotonation of surface functional groups), while the ionic strength can suppress electrostatic interaction and enhance hydrophobic–hydrophobic interaction [42,43].

Preliminary investigation of the effect of pH on the dye (without addition of adsorbent) was carried out in our previous work [13]. These data were useful to find the range of pH suitable for the study of adsorption activity of MG, as well as avoiding pH ranges that could lead to error. Briefly, major decolourisation of MG was found to occur at pH ≥ 8 due to alkaline fading, and at pH ≤ 2.0 due to formation of MG-H^{2+} species, while at pH 7, 20% reduction in colour intensity was observed [13,44]. Therefore, the adsorption study on the effect of pH experiment was limited to a pH range from 3.0 to 6.5.

The effect of pH on adsorption studies of MG is summarised in Fig. 1(A). The effect of pH for all the three adsorbents was conducted at a dye concentration of 100 mg L^{-1}. The unadjusted pH of 100 mg L^{-1} MG was at 3.8. UAP and PAP exhibited a gradual increase of dye uptake until a maximum before the adsorption decreases, while NAP exhibited increase in dye removal with increasing pH without any decrease in adsorption beyond pH 5.0. The optimum pH for dye uptake for UAP, PAP and NAP were at 5.0, 5.0 and 5.9, respectively. However, it was observed that dye adsorption for UAP and NAP at unadjusted pH (q_e at

60.5 and 89.2 mg g^{-1}, respectively) was comparable with the optimum pH (q_e at 64.6 and 94.4 mg g^{-1}). Hence, it was decided that unadjusted pH is more economical and was thus applied to the rest of the experiment involving UAP and NAP, whereas for PAP all experiments were conducted at pH 5.0.

The point of zero charge (pH_{pzc}) is the pH where the net charge on the adsorbent surface is zero. The pH_{pzc} of UAP, PAP and NAP at adsorbent dosage of 0.03 g/20 mL dye was 5.3, 5.9 and 6.6, respectively. By the concept of pH_{pzc}, the surface of the adsorbent will be predominantly negatively charged when solution pH > pH_{pzc}, while net positive charge obtained when solution pH < pH_{pzc}. As the MG molecules are cationic below pH of 6.9 (pK_a 6.9), the dye molecules should engage in electrostatic repulsion with predominant positively charged adsorbent surface if the pH < pH_{pzc} and should result in a decrease of dye adsorption. However, this was not observed for all the three adsorbents. As described above, the dye adsorption of NAP increased very slightly as pH increased from 3.0 to 6.5, while UAP and PAP exhibited an increase in dye adsorption with increasing pH, but it decreased when pH > pH_{pzc} (Fig. 1(A)). The disagreement of the experimental data with pH_{pzc} concept merely indicated that the adsorption of MG by these adsorbents is not purely by electrostatic attraction, while the hydrophobic–hydrophobic interaction and hydrogen bonding may be significantly dominant. Similar observations were reported by Al-Degs et al. [43].

The effect of ionic strength was studied under various concentrations of KNO_3 and NaCl salt solutions with dye concentration of 100 mg L^{-1} and the result is summarised in Fig. 1(B) and (C). As salt concentration is directly proportionally to ionic strength, an increase in salt concentration will increase the ionic strength of the solution. All the three adsorbents showed some decrease in dye adsorption as the ionic strength increases. From no addition of salt to 0.8 mol L^{-1} salt solution, UAP, PAP and NAP displayed 14.4, 35.4 and 25.0% reduction in dye adsorption in KNO_3 solution, whereas for NaCl solution displayed a reduction of 7.1, 40.9 and 26.1%, respectively. As reported by Hu et al., cationic dye adsorption decreases when there is an increase in ionic strength, while the reverse is observed for anionic dye [42], which is in full agreement with our data as shown in Fig. 1(B) and (C). The reduction of q_e is due to the suppression of electrostatic interaction as high concentrations of Na^+ and K^+ compete with MG molecules for the adsorption sites on the adsorbent's surface [42,45]. The reduction in adsorption at high salt content may hint the amount of dye interaction occurred via electrostatic attraction.
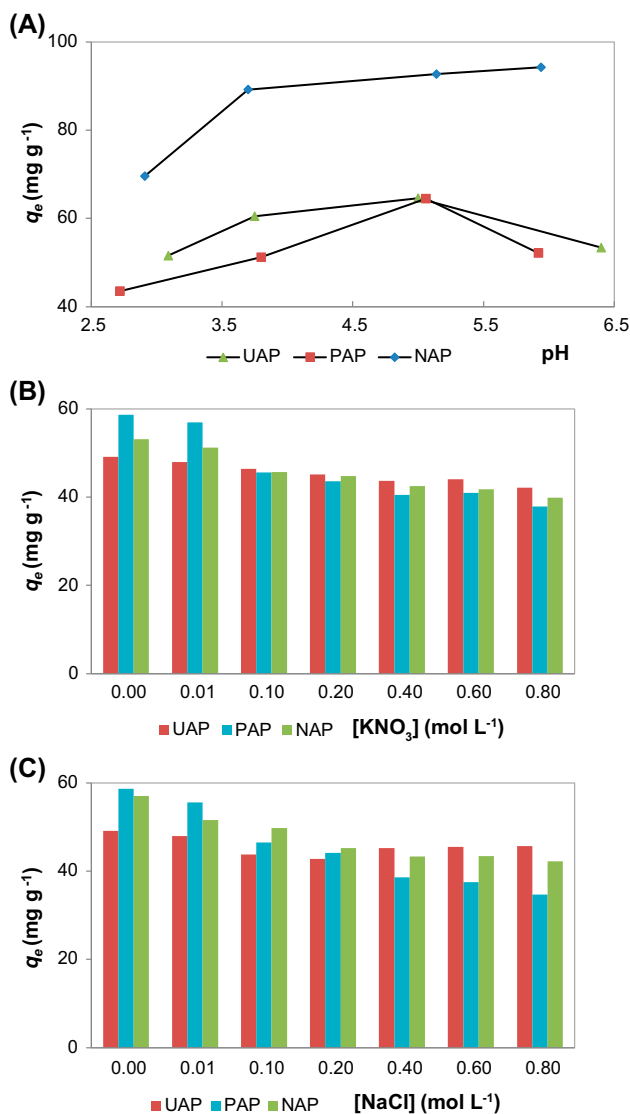
Fig. 1. (A) Effects of pH with C_i at 100 mg L^{-1} for UAP and NAP, and 400 mg L^{-1} for PAP, and the effect of ionic strength at various concentrations of (B) KNO_3 and (C) NaCl, on the removal of 100 mg L^{-1} MG for all three adsorbents, at dosage of 0.03 g adsorbent in 20 mL dye.

This feature of unmodified and chemical-modified AP to maintain high adsorption despite high salt concentration is also advantageous in situations such as the treatment of textile dye effluents or dye-contaminated fish wastewater, where the salt content can be high.

3.4. Effect of contact time and kinetics modelling

Determination of the contact time is essential in adsorption studies as it ensures that the equilibrium of the adsorbent–dye system is attained. The effects of contact time are summarised in Fig. 2. All plots exhibit similar behaviour where the dye uptake was high at the early stage of the adsorption and slowing down to almost a plateau at the end. The rapid dye uptake at the initial stage is due to the availability of vacant sites at the beginning of the adsorption process which gradually become scarce over time [46]. An agitation time of 180 min was deemed sufficient for all three adsorbent–dye systems to reach equilibrium, as little variation was observed beyond that time, and thus all experiments was agitated for 180 min.

To model the adsorption process, the experimental data were fitted to the following kinetics models: the pseudo-first-order [47], pseudo-second-order [48], Weber–Morris intraparticle diffusion [49] and Boyd [50] kinetics models.

The pseudo-first-order equation is an approximate solution to first-order rate mechanism, and it is commonly used for modelling sorption process in liquid–solid system based on the capacity of the solid [51]. The equation of the pseudo-first-order is expressed as:

$$\log(q_e - q_t) = \log\, q_e - \frac{t}{2.303} k_1 \tag{5}$$

where q_t is the amount of adsorbate adsorbed per gram of adsorbent (mg g^{-1}) at time t, k_1 is the pseudo-first-order rate constant (min^{-1}) and t is the time shaken (min).

The pseudo-second-order is a chemisorption kinetics model which assumes the adsorption reaction on adsorbent surface is the rate-limiting step. Hence, the adsorption process followed rate law of a second-order kinetics with respect to the availability of adsorption sites on the adsorbent's surface instead of adsorbate concentration in bulk solution [52]. The equation is expressed as:

$$\frac{t}{q_t} = \frac{1}{q_e^2 k_2} + \frac{t}{q_e} \tag{6}$$
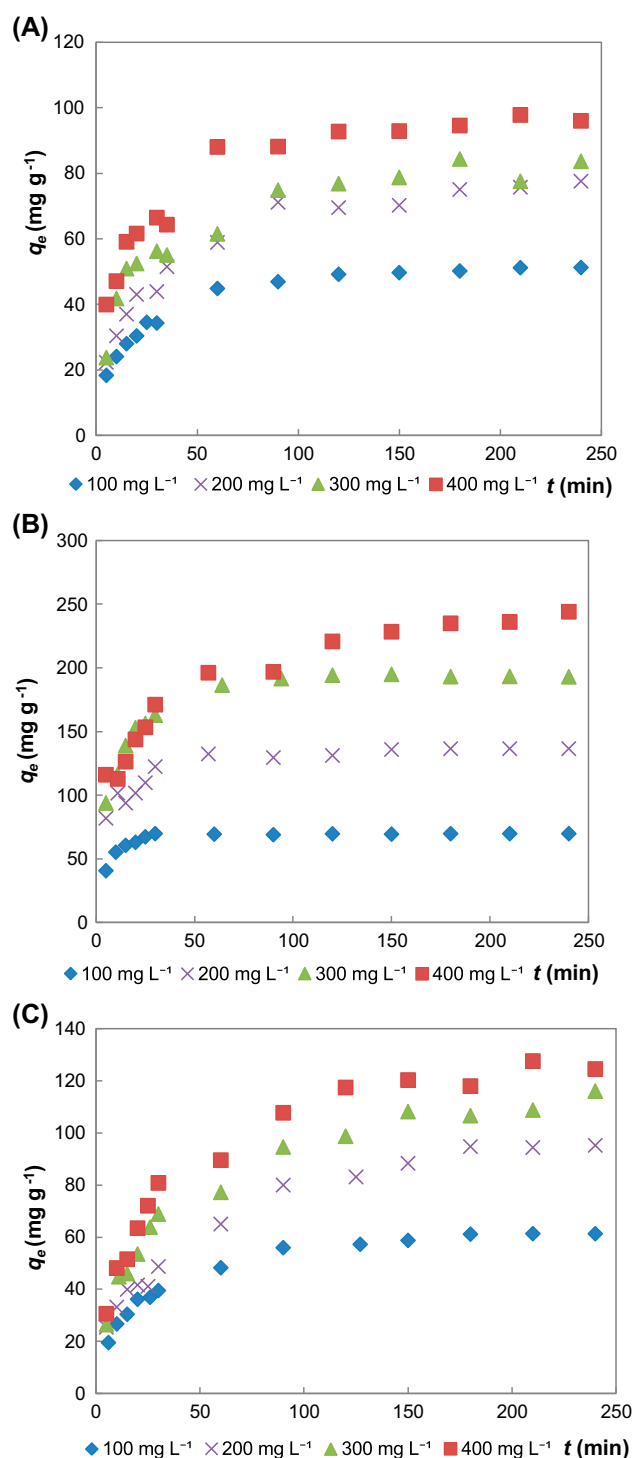
Fig. 2. Effect of contact time carried out at C_i 100, 200, 300 and 400 mg L^{-1} for adsorbent (A) UAP, (B) PAP and (C) NAP.

where k_2 is pseudo-second-order rate constant (g mg^{-1} min^{-1}).

The parameters of the pseudo-first-order and pseudo-second-order were calculated from the linear plot of $\ln(q_e - q_t)$ vs. t, and t/q_t vs. t respectively, and are summarised in Table 2 and Fig. 3(A)–(C) (pseudo-first-order plots not shown for brevity). The values of the coefficient of determination, R^2, of pseudo-second-order are much closer to 1.0 than the pseudo-first-order for all the three adsorbents. Error functions χ^2, EABS, ARE and MSDP of the pseudo-second-order for all the three adsorbents were much lower than the pseudo-first-order, where smaller values indicate smaller error. Lastly, by comparing the experiment q_e ($q_{e,exp}$) to the calculated q_e ($q_{e,cal}$), where both values were much closer for pseudo-second-order than pseudo-first-order. Thus by considering the R^2, error functions and the comparison of $q_{e,exp}$ and $q_{e,cal}$, it is concluded that the pseudo-second-order best represented the adsorption process of all the three adsorbents.

To investigate diffusion mechanism, the Weber–Morris intraparticle diffusion and Boyd models were employed, as the two previous kinetics models were not applicable.

The Weber–Morris intraparticle diffusion model is expressed:

$$q_t = k_3 t^{1/2} + C \tag{7}$$

where k_3 is the intraparticle diffusion rate constant (mg g^{-1} min$^{-1/2}$) and C is the intercept that represents the thickness of the boundary layer. These parameters were obtained from the linear plot of q_t vs. $t^{1/2}$.

Generally, intraparticle diffusion model are divided into three phases. The first phase is the fast external surface adsorption, followed by intraparticle diffusion phase and the slow equilibrium phase of remaining [53,54]. The Weber–Morris plots are shown

Table 2
Summary of all the parameters of various kinetics models of all three adsorbents

| Adsorbent | Pseudo-first-order model | | | | | | | | | | | |
	UAP				PAP				NAP			
C_i (mg L^{-1})	100	200	300	400	100	200	300	400	100	200	300	400
$q_{e,cal}$ (mg g^{-1})	35.7	50.0	47.6	46.5	11.7	60.5	51.3	130.6	60.6	93.0	91.5	86.3
$q_{e,exp}$ (mg g^{-1})	51.3	77.6	84.4	97.8	70.0	136.7	195.0	244.2	61.4	95.3	108.9	127.6
k_1	0.025	0.016	0.014	0.015	0.030	0.032	0.019	0.014	0.030	0.022	0.024	0.015
R^2	0.929	0.954	0.882	0.939	0.882	0.880	0.731	0.987	0.930	0.908	0.876	0.942
χ^2	88	173	272	407	544	568	1,228	828	15	23	64	259
EABS	191	322	433	592	619	841	1,474	1,234	54	72	195	488
ARE	42	51	58	64	75	57	71	57	14	14	26	50
MSDP	53	63	71	78	98	76	93	77	24	27	38	62
Pseudo-second-order model												
$q_{e,cal}$ (mg g^{-1})	54.3	82.7	87.1	101.7	70.7	140.1	199.8	253.5	66.1	106.8	120.4	137.8
$q_{e,exp}$ (mg g^{-1})	51.3	77.6	84.4	97.8	70.0	136.7	195.0	244.2	61.4	95.3	108.9	127.6
k_2	0.0013	0.0006	0.0008	0.0008	0.0071	0.0013	0.0009	0.0003	0.0009	0.0003	0.0004	0.0003
R^2	1.000	0.997	0.995	0.998	1.000	1.000	1.000	0.998	0.999	0.993	0.996	0.995
χ^2	25	3	5	6	32	6	2	23	30	8	3	5
EABS	87	31	46	43	72	61	45	87	108	49	34	47
ARE	19	6	6	6	11	5	2	5	20	9	5	6
MSDP	26	10	9	10	28	8	4	15	26	15	9	10
Weber–Morris intraparticle diffusion model[a]												
k_3	5.2	7.3	7.9	7.1	8.5	10.7	22.2	17.9	6.4	6.5	12.6	14.9
C	7.5	7.3	13.5	26.6	25.4	58.6	46.9	64.8	5.4	12.3	−0.7	−2.5
R^2	0.977	0.953	0.800	0.883	0.941	0.841	0.961	0.852	0.964	0.931	0.979	0.982
Boyd model[a]												
Slope	0.020	0.016	0.018	0.015	0.073	0.050	0.041	0.015	0.019	0.016	0.018	0.018
Y-Intercept	0.047	−0.107	−0.025	0.246	0.384	0.072	0.057	0.103	−0.073	−0.242	−0.176	−0.192
R^2	0.978	0.995	0.985	0.939	0.949	0.954	0.990	0.988	0.983	0.989	0.977	0.987

[a]Represented the calculated parameters derived from the first linear region.
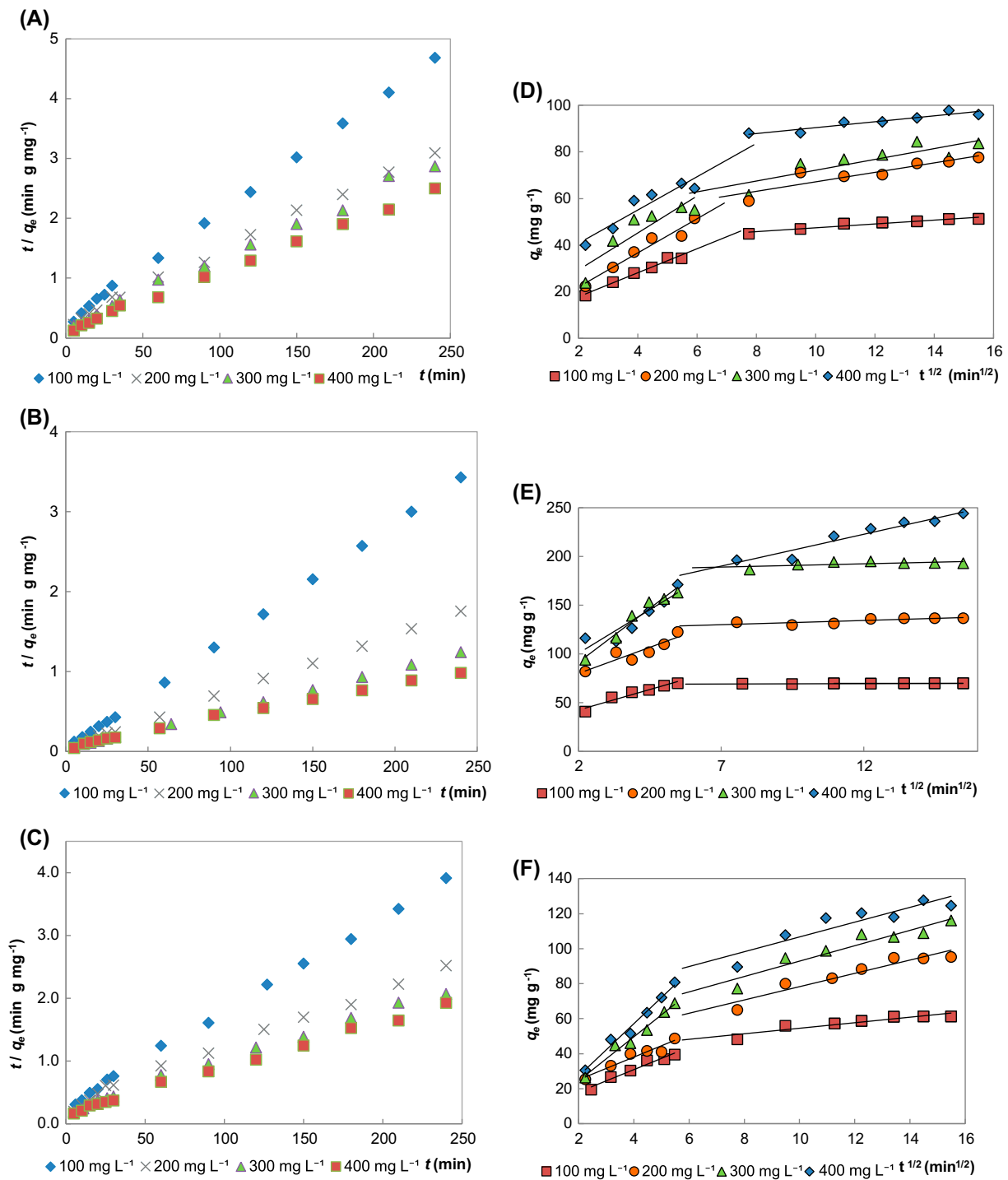
Fig. 3. Pseudo-second-order plots of (A) UAP, (B) PAP and (C) NAP and the Weber–Morris plots of (D) UAP, (E) PAP, and (F) NAP.

in Fig. 3(D)–(F), where the plots exhibit multilinearity. The fast adsorption phase was completed within 5 min and was not observed in the plot. This behaviour was reported in other research works [53,54]. The first linear region in the Weber–Morris plots

represented the intraparticle diffusion phase, while the second region represented the slow equilibrium phase.

According to the Weber–Morris intraparticle diffusion model, if the linear plot crosses the origin, then the intraparticle diffusion phase is the rate-limiting

phase. As the C for all the three adsorbent–dye systems are non-zero, the data indicate that intraparticle diffusion is not the rate-limiting step for all the three dye–adsorbent systems, and other mechanisms may be involved.

The Boyd model is typically expressed as:

$$B_t = -0.4977 - \ln(1 - F) \quad (8)$$

where F is equivalent to q_t/q_e which represents the fraction of adsorbate adsorbed at different times, and B_t is mathematical function of F.

According to the Boyd model, if the linear plot of B_t vs. t (plot not showed for brevity) crossed the origin, then the diffusion process is controlled by particle diffusion, and if the plot intersect is non-origin then it is film diffusion [55]. Film diffusion is the transfer of adsorbates to the external surface of the adsorbent particles, while particle diffusion is the transfer of adsorbates into the pores of the adsorbents. As seen in Table 2, all the adsorbents displayed non-zero intersections thus suggesting that the rate-limiting step for all three adsorbents may be controlled by film diffusion.

3.5. Effect of concentration and isotherm modelling

The effect of C_i under different temperatures is summarised in Fig. 4. For UAP and NAP, the dye uptake increased with increasing concentration. This behaviour can be explained with the higher driving force resulted from higher C_i that drive the dye molecules deeper into the micro-pores of the adsorbents [46]. However, when the C_i is beyond 200 mg L^{-1}, the adsorption varied slightly. This is due to the adsorbent reaching the maximum capacity of dye uptake. For PAP, the upward trend of the dye adsorption with increasing concentration is due to higher dye uptake capacity. For all the three adsorbents, higher temperature only slightly improves the dye uptake.

The adsorption process was described with three adsorption isotherm models: Langmuir [56], Freundlich [57] and Dubinin–Radushkevich (D–R) [58].

The Langmuir model assumes homogeneous adsorption resulting in monolayer, where no further adsorption can occur when a site is occupied with adsorbate. The equation is expressed as:

$$\frac{C_e}{q_e} = \frac{1}{K_L q_m} + \frac{C_e}{q_m} \quad (9)$$
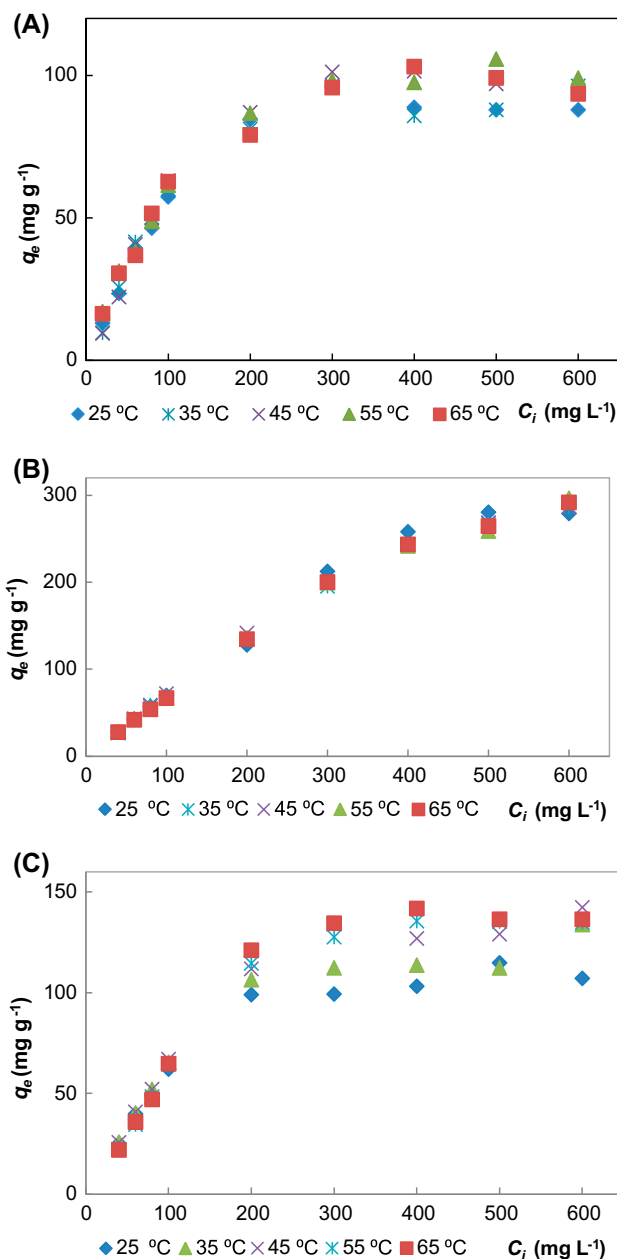
Fig. 4 Effect of concentration for (A) UAP, (B) PAP and (C) NAP, under different temperatures.

where q_m is the maximum monolayer adsorption capacity of the adsorbent (mg g^{-1}), and K_L is the Langmuir adsorption constant (L mg^{-1}) which is related to the free energy of adsorption.

The separation factor (R_L) is a dimensionless constant which is an essential characteristic of the Langmuir model. The equation of R_L is expressed as:

$$R_L = \frac{1}{(1 + K_L C_o)} \tag{10}$$

where C_o (mg L^{-1}) is the highest initial dye concentration. R_L indicates if the isotherm is unfavourable ($R_L > 1$), linear ($R_L = 1$), favourable ($0 < R_L < 1$) or irreversible ($R_L = 0$).

The Freundlich isotherm model assumes multilayers adsorption, where further adsorption is possible on the adsorbate-saturated adsorbent's surface. The equation is expressed as:

$$\ln q_e = \frac{1}{n_F} \ln C_e + \ln K_F \tag{11}$$

where K_F (mg$^{1-1/n}$ L$^{1/n}$ g^{-1}) is the adsorption capacity of the adsorbent and n_F (Freundlich constant) indicates the favourability of the adsorption process. The adsorption process is considered favourable if $1 < n_F < 10$.

The D–R isotherm is similar to the Langmuir model, however it does not assume homogenous surface and is temperature-dependent. The equation is as followed:

$$\ln q_e = \ln q_m - K_{DR}\varepsilon^2 \tag{12}$$

where q_m is the saturation capacity (mg g^{-1}), K_{DR} is a D–R constant (mol^2 kJ^{-2}), and is the D–R isotherm constant.

The D–R isotherm constant, ε, is expressed as:

$$\varepsilon = RT \ln\left[1 + \frac{1}{C_e}\right] \tag{13}$$

where R is the gas constant (8.314×10^{-3} kJ mol^{-1} K^{-1}) and T is temperature (K).

The mean free energy, E (kJ mol^{-1}), of the sorption per molecule of adsorbate is obtained from K_{DR}, and the equation is expressed as:

$$E = \frac{1}{\sqrt{2K_{DR}}} \tag{14}$$

The parameters for the Langmuir, Freundlich and D–R isotherm models were obtained through the linear plots of C_e/q_e vs. C_e, $\ln q_e$ vs. $\ln C_e$, and $\ln q_e$ vs. ε^2, respectively, and are summarised in Table 3. The R^2 values for the Langmuir model is the highest compared to the Freundlich and D–R isotherm models. Generally, the values of the error analysis functions

(χ^2, EABS, ARE and MSDP) of the Langmuir model were also the lowest, indicating the least error. Therefore, the experimental data are best represented by the Langmuir model.

The values of R_L of all the adsorbents for all the temperatures are between 0 and 1. This indicates the adsorption process between the adsorbents and MG is favourable. The lower values of K_F of Freundlich isotherm and q_m of D–R isotherm are due to experiment data being less fitted to these models.

Among the AP samples, PAP displayed the highest q_m at 292.1 mg g^{-1} at 25°C, followed by NAP and UAP at 109.6 and 87.0 mg g^{-1}, respectively. The comparison of q_m with other reported adsorbents for removal of MG is summarised in Table 4. PAP is a much better adsorbent than many studied samples, while NAP and UAP are average in the list.

3.6. Thermodynamics studies

The thermodynamics studies for the adsorption process were investigated at temperatures ranging from 25 to 65°C. The thermodynamics parameters were obtained with the following equations:

$$\Delta G° = \Delta H° - T\Delta S° \tag{15}$$

$$\Delta G° = -RT \ln k \tag{16}$$

$$k = \frac{C_s}{C_e} \tag{17}$$

$$\ln K = \frac{\Delta S°}{R} - \frac{\Delta H°}{RT} \tag{18}$$

where $\Delta G°$ is the Gibbs-free energy, $\Delta H°$ is the change in enthalpy, $\Delta S°$ is the change in entropy, T is the temperature (K), k is the distribution coefficient for adsorption, C_S is the concentration of dye adsorbed by the adsorbent at equilibrium (mg L^{-1}), C_e is the concentration of dye remains in solution at equilibrium (mg L^{-1}), R is the gas constant (J mol^{-1} K^{-1}) and T is the temperature (K).

The thermodynamics parameters are calculated from the linear plot of $\ln k$ vs. T^{-1}. Increasing temperature resulted in the Gibbs energy becoming less positive for all three adsorbent–MG systems. This behaviour indicates the improvement of spontaneity of the MG adsorption system with increasing temperature [64]. The $\Delta H°$ of UAP, PAP and NAP are 9.6, 19.2 and 30.0 kJ mol^{-1}, respectively. The positive values of $\Delta H°$ indicated that the reactions of these dye–adsorbent systems are endothermic. The $\Delta S°$ of UAP, PAP

Table 3
Parameters of various isotherm models for UAP and chemical-modified adsorbents

Langmuir isotherm

	UAP					PAP					NAP				
T (℃)	25	35	45	55	65	25	35	45	55	65	25	35	45	55	65
q_m	87.0	88.6	94.3	97.8	97.3	292.1	294.0	294.3	295.7	298.1	109.6	123.8	138.6	136.9	140.3
K_L	0.165	0.158	0.345	0.203	0.256	0.125	0.149	0.132	0.136	0.126	0.142	0.109	0.181	0.235	0.321
R_L	0.010	0.010	0.005	0.009	0.006	0.013	0.011	0.012	0.012	0.013	0.012	0.014	0.009	0.007	0.005
R^2	0.998	0.996	0.998	0.998	0.997	0.999	0.998	0.998	0.993	0.996	0.997	0.988	0.996	1.000	1.000
χ^2	7	13	9	19	10	12	21	37	42	46	5	35	19	6	7
EABS	43	54	52	62	58	67	105	140	170	160	40	114	84	35	52
ARE	10	16	10	17	12	11	14	18	18	22	8	22	15	8	10
MSDP	14	30	16	30	18	18	24	27	27	35	13	33	22	15	16

Freundlich isotherm

K_F	19.2	23.3	23.4	29.8	28.0	43.7	49.5	48.0	49.9	47.5	31.0	36.2	39.6	35.9	36.3
n_F	3.28	3.81	3.65	4.43	4.37	2.48	2.52	2.55	2.61	2.50	4.36	4.54	4.31	3.95	3.86
R^2	0.905	0.881	0.817	0.928	0.817	0.905	0.839	0.796	0.810	0.790	0.907	0.876	0.859	0.838	0.825
χ^2	36	25	27	12	170	75	108	129	112	53	13	19	28	37	10
EABS	133	113	115	74	216	283	326	351	322	181	73	92	130	138	76
ARE	21	22	20	13	56	24	29	32	30	25	12	15	19	22	10
MSDP	27	30	25	19	97	33	42	47	45	41	18	23	28	32	14

Dubinin–Radushkevich isotherm

q_m	63.5	67.7	78.3	76.1	85.7	226.5	229.8	245.1	247.7	244.6	88.0	103.9	123.3	125.2	128.8
k_{DR}	0.421	0.113	0.241	0.135	0.627	0.868	0.682	0.911	0.715	0.809	0.825	0.668	0.568	0.596	0.578
E	1.090	2.106	1.441	1.924	0.893	0.759	0.857	0.741	0.836	0.786	0.779	0.865	0.938	0.916	0.930
R^2	0.677	0.772	0.810	0.740	0.894	0.942	0.944	0.984	0.969	0.916	0.761	0.888	0.966	0.979	0.972
χ^2	77	88	46	64	170	78	40	16	22	53	41	23	9	30	10
EABS	195	187	151	181	216	241	211	122	139	181	149	108	76	122	76
ARE	35	35	28	29	56	15	18	9	12	25	24	16	10	18	10
MSDP	48	55	37	39	97	27	22	12	17	41	31	22	13	25	14

Table 4
Comparison of maximum adsorption capacity of various adsorbents under different conditions for the removal of MG

Adsorbent	q_m (mg g^{-1})	pH	T (℃)	Adsorbent dosage (g/100 mL dye)	Refs.
Arunda donax root carbon	8.7	5	30	0.60	[59]
NaOH-modified rice husk	15.5	7	30	1.00	[34]
Caulerpa racemosa	29.9	Unadjusted	25	0.40	[60]
Corn cob	80.6	8	27	0.40	[61]
UAP	87.0	Unadjusted	25	0.15	This work
Activated carbon-CoFe$_2$O$_4$ composites	89.3	5	25	0.20	[62]
Walnut shell	90.8	Unadjusted	25	0.15	[13]
NAP	109.6	Unadjusted	25	0.15	This work
Pithophora sp.	117.6	5	30	0.10	[63]
Peat	143.7	Unadjusted	25	0.20	[26]
Breadnut peel	177.4	Unadjusted	25	0.20	[35]
PAP	292.1	5	25	0.15	This work
NaOH-modified breadnut peel	353.0	Unadjusted	25	0.20	[35]

and NAP are 34.1, 93.5 and 108.1 J mol^{-1} K^{-1}, respectively, where the positive entropy indicates an increasing in randomness of adsorbates in the solid–liquid interface, resulted in desorption of water molecules from the adsorbent's surface [65].

The activation energy of the adsorption process was investigated with the Arrhenius equation which is expressed as:

$$\ln \; k_2 = \ln \; A - \frac{E_a}{RT} \tag{19}$$

where k_2 is the pseudo-second-order rate constant (g mg^{-1} min^{-1}), A is the Arrhenius factor, R is the gas constant, T is temperature (K) and E_a is the activation energy (kJ mol^{-1}).

The values of k_2 are obtained from kinetics experiment of dye C_i 100 mg L^{-1} carried out at temperatures 25, 35, 45, 55 and 65℃. The Arrhenius plot is as shown in Fig. 5. The E_a is obtained from the linear plot of ln k_2 vs. T^{-1}. E_a with values ranged from 5 to 40 kJ mol^{-1} may indicate physisorption-dominant process, while 40 to 800 kJ mol^{-1} indicates a predominantly chemisorption process [60]. The E_a obtained from UAP, PAP and NAP are 32.3, 58.7 and 34.1 kJ mol^{-1}, respectively. Therefore, UAP and NAP may operate dominantly by physisorption, while PAP may attribute more towards chemisorption.

3.7. Regeneration experiment

The distilled water and acid washing displayed gradual reduction in adsorption capacities for all the adsorbents with every proceeding cycle. NaOH
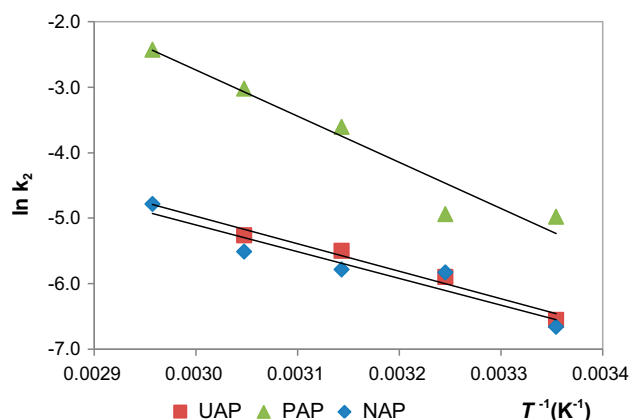
washing led to a better adsorption capacity as observed for UAP. This behaviour can be reasoned by the removal of natural fats, waxes and low-molecular weight lignin compounds from the surface of the adsorbent by the base, leading to the exposure of chemical-reactive functional groups, such as the hydroxyl groups, which may be responsible for removal of MG [34]. For PAP and NAP, the basic wash did not regenerate the adsorption capacity to the former level, unlike UAP. At the fifth cycle, the removal capacities of UAP, PAP and NAP by basic wash are at 44.1, 45.3 and 52.6 mg g^{-1}, as compared to the original level at 40.6, 68.3 and 58.5 mg g^{-1}, respectively.

4. Conclusions

The potential of AP and modified AP for the removal of MG was studied in batch adsorption system. PAP showed higher dye removal, followed by NAP and UAP. Kinetics modelling suggested all the three adsorbents are best represented by the pseudo-second-order. The Weber–Morris model showed that intraparticle diffusion is not the rate-limiting step for all three MG-adsorbent systems, and the Boyd model suggested that film diffusion may be the rate-limiting step. The Langmuir isotherm best represented these three adsorption systems, with q_m at 87.0, 292.1 and 109.6 mg g^{-1} at 25℃ for UAP, PAP and NAP, respectively. Thermodynamics studies showed that all the three adsorption systems are spontaneous and endothermic. Estimation of activation energy by the Arrhenius equation suggested UAP and NAP might be operated by physisorption, while PAP might be operated dominantly by chemisorption. Regeneration experiment showed that 0.1 mol L^{-1} NaOH is capable of regenerating the adsorbent, and is effective even after the fifth cycle.

Fig. 5. Arrhenius plot of the AP adsorbents in removal of MG.

References

[1] A. Mittal, Adsorption kinetics of removal of a toxic dye, Malachite Green, from wastewater by using hen feathers, J. Hazard. Mater. 133 (2006) 196–202.

[2] Z. Bajc, V. Jenčič, K. Šinigoj, Gačnik, Elimination of malachite green residues from meat of rainbow trout and carp after water-born exposure, Aquaculture 321 (2011) 13–16.

[3] R. Liu, W. Hei, P. He, Z. Li, Simultaneous determination of fifteen illegal dyes in animal feeds and poultry products by ultra-high performance liquid chromatography tandem mass spectrometry, J. Chromatogr., B 879 (2011) 2416–2422.

[4] SIGMA-ALDRICH, Malachite green oxalate salt [Material Safety Data Sheet] Version 5.0, Retrieved from: <http://www.sigmaaldrich.com/MSDS/MSDS/DisplayMSDSPage.do?country=BN&language=EN-generic&productNumber=M9015&brand=SIGMA> (21 May 2015).

[5] I.M. Banat, P. Nigam, D. Singh, R. Marchant, Microbial decolorization of textile-dyecontaining effluents: A review, Bioresour. Technol. 58 (1996) 217–227.

[6] C. Moran, M. Hall, R. Howell, Effects of sewage treatment on textile effluent, J. Soc. Dyers Colour. 113 (1997) 272–274.

[7] R.N. Goyal, A. Kumar, A. Mittal, Oxidation chemistry of adenine and hydroxyadenines at pyrolytic graphite electrodes, J. Chem. Soc., Perkin Trans. 2(9) (1991) 1369–1375.

[8] M. Naushad, A. Mittal, M. Rathore, V. Gupta, Ion-exchange kinetic studies for Cd(II), Co(II), Cu(II), and Pb(II) metal ions over a composite cation exchanger, Desalin. Water Treat. 54 (2014) 2883–2890.

[9] T. Robinson, G. McMullan, R. Marchant, P. Nigam, Remediation of dyes in textile effluent: A critical review on current treatment technologies with a proposed alternative, Bioresour. Technol. 77 (2001) 247–255.

[10] A. Srinivasan, T. Viraraghavan, Decolorization of dye wastewaters by biosorbents: A review, J. Environ. Manage. 91 (2010) 1915–1929.

[11] Z. Wang, M. Xue, K. Huang, Z. Liu, Textile dyeing wastewater treatment, in: P.J. Hauser (Ed.), Advances in Treating Textile Effluent, InTech, Rijeka, 2011, pp. 5–116.

[12] G. Crini, Non-conventional low-cost adsorbents for dye removal: A review, Bioresour. Technol. 97 (2006) 1061–1085.

[13] M.K. Dahri, M.R.R. Kooh, L.B.L. Lim, Water remediation using low cost adsorbent walnut shell for removal of malachite green: Equilibrium, kinetics, thermodynamic and regeneration studies, J. Environ. Chem. Eng. 2 (2014) 1434–1444.

[14] H. Daraei, A. Mittal, J. Mittal, H. Kamali, Optimization of Cr(VI) removal onto biosorbent eggshell membrane: experimental & theoretical approaches, Desalin. Water Treat. 52 (2013) 1307–1315.

[15] H. Daraei, A. Mittal, M. Noorisepehr, J. Mittal, Separation of chromium from water samples using eggshell powder as a low-cost sorbent: Kinetic and thermodynamic studies, Desalin. Water Treat. 53 (2013) 214–220.

[16] A. Mittal, Use of hen feathers as potential adsorbent for the removal of a hazardous dye, Brilliant Blue FCF, from wastewater, J. Hazard. Mater. 128 (2006) 233–239.

[17] A. Mittal, J. Mittal, Hen feather: A remarkable adsorbent for dye removal, in: S.K. Sharma (Ed.), Green Chemistry for Dyes Removal from Wastewater, Scrivener Publishing LLC, Salem, Massachusetts, 2015, pp. 409–457.

[18] J. Mittal, V. Thakur, A. Mittal, Batch removal of hazardous azo dye Bismark Brown R using waste material hen feather, Ecol. Eng. 60 (2013) 249–253.

[19] A. Mittal, L. Kurup, Column operations for the removal and recovery of a hazardous dye 'acid red—27' from aqueous solutions, using waster materials-bottom ash and de-oiled soya, Ecol. Environ. Conserv. 12 (2006) 181–186.

[20] J. Mittal, D. Jhare, H. Vardhan, A. Mittal, Utilization of bottom ash as a low-cost sorbent for the removal and recovery of a toxic halogen containing dye eosin yellow, Desalin. Water Treat. 52 (2014) 4508–4519.

[21] G. Sharma, M. Naushad, D. Pathania, A. Mittal, G.E. El-desoky, Modification of *Hibiscus cannabinus* fiber by graft copolymerization: Application for dye removal, Desalin. Water Treat. 54 (2014) 3114–3121.

[22] N. Priyantha, L.B.L. Lim, M.K. Dahri, Dragon fruit skin as a potential low-cost biosorbent for the removal of manganese(II) ions, J. Appl. Sci. Environ. Sanit. 8 (2013) 179–188.

[23] L.B.L. Lim, N. Priyantha, H.I. Chieng, M.K. Dahri, *Artocarpus camansi* Blanco (Breadnut) core as low-cost adsorbent for the removal of methylene blue: Equilibrium, thermodynamics, and kinetics studies, Desalin. Water Treat. (in press) 1–13, doi: 10.1080/19443994.2015.1007088.

[24] L.B.L. Lim, N. Priyantha, D.T.B. Tennakoon, M.K. Dahri, Biosorption of cadmium(II) and copper(II) ions from aqueous solution by core of *Artocarpus odoratissimus*, Environ. Sci. Pollut. Res. 19 (2012) 3250–3256.

[25] L.B.L. Lim, N. Priyantha, N.H.M. Mansor, *Artocarpus altilis* (breadfruit) skin as a potential low-cost biosorbent for the removal of crystal violet dye: Equilibrium, thermodynamics and kinetics studies, Environ. Earth Sci. 73 (2014) 3239–3247.

[26] H.I. Chieng, T. Zehra, L.B.L. Lim, N. Priyantha, D.T.B. Tennakoon, Sorption characteristics of peat of Brunei Darussalam IV: Equilibrium, thermodynamics and kinetics of adsorption of methylene blue and malachite green dyes from aqueous solution, Environ Earth Sci. 72 (2014) 2263–2277.

[27] P. Leterme, A.M. Londoño, J.E. Muñoz, J. Súarez, C.A. Bedoya, W.B. Souffrant, A. Buldgen, Nutritional value of aquatic ferns (*Azolla filiculoides* Lam. and *Salvinia molesta* Mitchell) in pigs, Anim. Feed Sci. Technol. 149 (2009) 135–148.

[28] A.B. Albadarin, A.a.H. Al-Muhtaseb, G.M. Walker, S.J. Allen, M.N.M. Ahmad, Retention of toxic chromium from aqueous phase by H_3PO_4-activated lignin: Effect of salts and desorption studies, Desalination 274 (2011) 64–73.

[29] P.K. Rai, Technical note: Phytoremediation of Hg and Cd from industrial effluents using an aquatic free

floating macrophyte *Azolla pinnata*, Int. J. Phytorem. 10 (2008) 430–439.

[30] S. Jain, P. Vasudevan, N. Jha, *Azolla pinnata* r.br. and *Lemna minor* l. for removal of lead and zinc from polluted water, Water Res. 24 (1990) 177–183.

[31] J.P. Gaur, N. Noraho, Adsorption and uptake of cadmium by *Azolla pinnata*: Kinetics of inhibition by cations, Biomed. Environ. Sci. 8 (1995) 149–157.

[32] M.R.R. Kooh, L.B.L. Lim, M.K. Dahri, L.H. Lim, J.M.R. Sarath Bandara, *Azolla pinnata*: An efficient low cost material for removal of methyl violet 2B by using adsorption method, Waste Biomass Valor. (in press), doi: 10.1007/s12649-015-9369-0.

[33] B.S. Girgis, M.F. Ishak, Activated carbon from cotton stalks by impregnation with phosphoric acid, Mater. Lett. 39 (1999) 107–114.

[34] S. Chowdhury, R. Mishra, P. Saha, P. Kushwaha, Adsorption thermodynamics, kinetics and isosteric heat of adsorption of malachite green onto chemically modified rice husk, Desalination 265 (2011) 159–168.

[35] H.I. Chieng, L.B. Lim, N. Priyantha, Enhancing adsorption capacity of toxic malachite green dye through chemically modified breadnut peel: Equilibrium, thermodynamics, kinetics and regeneration studies, Environ. Technol. 36 (2015) 86–97.

[36] T. Zehra, N. Priyantha, L.B.L. Lim, E. Iqbal, Sorption characteristics of peat of Brunei Darussalam V: Removal of Congo red dye from aqueous solution by peat, Desalin. Water Treat. 54 (2015) 2592–2600, doi: 10.1080/19443994.2014.899929.

[37] S.C. Tsai, K.W. Juang, Comparison of linear and non-linear forms of isotherm models for strontium sorption on a sodium bentonite, J. Radioanal. Nucl. Chem. 243 (2000) 741–746.

[38] L.B.L. Lim, N. Priyantha, C. Hei Ing, M. Khairud Dahri, D.T.B. Tennakoon, T. Zehra, M. Suklueng, *Artocarpus odoratissimus* skin as a potential low-cost biosorbent for the removal of methylene blue and methyl violet 2B, Desalin. Water Treat. 53 (2015) 964–975.

[39] H.I. Chieng, L.B.L. Lim, N. Priyantha, Sorption characteristics of peat from Brunei Darussalam for the removal of rhodamine B dye from aqueous solution: Adsorption isotherms, thermodynamics, kinetics and regeneration studies, Desalin. Water Treat. 55 (2015) 664–677, doi: 10.1080/19443994.2014.919609.

[40] L.B.L. Lim, N. Priyantha, D.T.B. Tennakoon, H.I. Chieng, M.K. Dahri, M. Suklueng, Breadnut peel as a highly effective low-cost biosorbent for methylene blue: Equilibrium, thermodynamic and kinetic studies, Arab. J. Chem. (in press), doi: 10.1016/j.arabjc.2013.12.018.

[41] R.K. Xu, S.C. Xiao, J.H. Yuan, A.Z. Zhao, Adsorption of methyl violet from aqueous solutions by the bio-chars derived from crop residues, Bioresour. Technol. 102 (2011) 10293–10298.

[42] Y. Hu, T. Guo, X. Ye, Q. Li, M. Guo, H. Liu, Z. Wu, Dye adsorption by resins: Effect of ionic strength on hydrophobic and electrostatic interactions, Chem. Eng. J. 228 (2013) 392–397.

[43] Y.S. Aldegs, M.I. Elbarghouthi, A.H. Elsheikh, G.M. Walker, Effect of solution pH, ionic strength, and temperature on adsorption behavior of reactive dyes on activated carbon, Dyes Pigm. 77 (2008) 16–23.

[44] B. Samiey, A.R. Toosi, Adsorption of malachite green on silica gel: Effects of NaCl, pH and 2-propanol, J. Hazard. Mater. 184 (2010) 739–745.

[45] V.J.P. Vilar, C.M.S. Botelho, R.A.R. Boaventura, Influence of pH, ionic strength and temperature on lead biosorption by Gelidium and agar extraction algal waste, Proc. Biochem. 40 (2005) 3267–3275.

[46] V.S. Mane, P. Babu, Studies on the adsorption of Brilliant Green dye from aqueous solution onto low-cost NaOH treated saw dust, Desalination 273 (2011) 321–329.

[47] S. Lagergren, Zur Theorie der Sogenannten Adsorption gel Ster Stoffe (About the theory of so-called adsorption of soluble substances), K. Sven. Vetenskapsakad. Handl. 24 (1898) 1–39.

[48] Y.S. Ho, G. McKay, Pseudo-second order model for sorption processes, Proc. Biochem. 34 (1999) 451–465.

[49] W. Weber, J. Morris, Kinetics of adsorption on carbon from solution, J. Sanit. Eng. Div. 89 (1963) 31–60.

[50] G.E. Boyd, A.W. Adamson, L.S. Myers Jr., The exchange adsorption of ions from aqueous solutions by organic zeolites. II. Kinetics 1, J. Am. Chem. Soc. 69 (1947) 2836–2848.

[51] Y.S. Ho, J.C.Y. Ng, G. McKay, Kinetics of pollutant sorption by biosorbents: Review, Sep. Purif. Rev. 29 (2000) 189–232.

[52] Y. Liu, New insights into pseudo-second-order kinetic equation for adsorption, Colloids Surf., A 320 (2008) 275–278.

[53] M. Özacar, İ.A. Şengil, Application of kinetic models to the sorption of disperse dyes onto alunite, Colloids Surf., A 242 (2004) 105–113.

[54] Y. Zhao, Q. Yue, Q. Li, X. Xu, Z. Yang, X. Wang, B. Gao, H. Yu, Characterization of red mud granular adsorbent (RMGA) and its performance on phosphate removal from aqueous solution, Chem. Eng. J. 193–194 (2012) 161–168.

[55] T. Maiyalagan, S. Karthikeyan, Film-pore diffusion modeling for sorption of azo dye on to exfoliated graphitic nanoplatelets Indian, J. Chem. Technol. 20 (2013) 7–14.

[56.] I. Langmuir, The constitution and fundamental properties of solids and liquids. Part I. Solids, J. Am. Chem. Soc. 38 (1916) 2221–2295.

[57] H.M.F. Freundlich, Over the adsorption in solution, J. Phys. Chem. 57 (1906) 385–471.

[58] M.M. Dubinin, L.V. Radushkevich, Equation of the characteristic curve of activated charcoal, Proc. Acad. Sci. 55 (1947) 327.

[59] J. Zhang, Y. Li, C. Zhang, Y. Jing, Adsorption of malachite green from aqueous solution onto carbon prepared from *Arundo donax* root, J. Hazard. Mater. 150 (2008) 774–782.

[60] Z. Bekçi, Y. Seki, L. Cavas, Removal of malachite green by using an invasive marine alga *Caulerpa racemosa* var. cylindracea, J. Hazard. Mater. 161 (2009) 1454–1460.

[61] G.H. Sonawane, V.S. Shrivastava, Kinetics of decolourization of malachite green from aqueous medium by

maize cob (Zea maize): An agricultural solid waste, Desalination 247 (2009) 430–441.

[62] L. Ai, H. Huang, Z. Chen, X. Wei, J. Jiang, Activated carbon/CoFe$_2$O$_4$ composites: Facile synthesis, magnetic performance and their potential application for the removal of malachite green from water, Chem. Eng. J. 156 (2010) 243–249.

[63] K.V. Kumar, S. Sivanesan, V. Ramamurthi, Adsorption of malachite green onto *Pithophora* sp., a fresh water algae: Equilibrium and kinetic modelling, Proc. Biochem. 40 (2005) 2865–2872.

[64] M. Hajjaji, A. Beraa, Chromate adsorption on acid-treated and amines-modified clay, Appl. Water Sci. 5 (2014) 73–79.

[65] W. Ruixia, C. Jinlong, C. Lianlong, F. Zheng-hao, L. Ai-min, Z. Quanxing, Study of adsorption of lipoic acid on three types of resin, React. Funct. Polym. 59 (2004) 243–252.